J|A|C|S
ARTICLES
Published on Web 04/19/2002

Protein Structure Determination Using Long-Distance Constraints from Double-Quantum Coherence ESR: Study of T4 Lysozyme

Petr P. Borbat,[†] Hassane S. Mchaourab,[‡] and Jack H. Freed*,[†]

Contribution from the Baker Laboratory of Chemistry and Chemical Biology, Cornell University, Ithaca, New York 14853-1301, and Department of Molecular Physiology and Biophysics, Vanderbilt University School of Medicine, Nashville, Tennessee 37232

Received January 8, 2002. Revised Manuscript Received March 6, 2002

Abstract: We report the use of a novel pulsed ESR technique for distance measurement, based on the detection of double quantum coherence (DQC), which yields high quality dipolar spectra, to significantly extend the range of measurable distances in proteins using nitroxide spin-labels. Eight T4 lysozyme (T4L) mutants, doubly labeled with methanethiosulfonate spin-label (MTSSL), have been studied using DQC-ESR at 9 and 17 GHz. The distances span the range from 20 Å for the 65/76 mutant to 47 Å for the 61/135 mutant. The high quality of the dipolar spectra also allows the determination of the distance distributions, the width of which can be used to set upper and lower bounds in future computational strategy. It is also demonstrated that the shape of these distributions can reveal the presence of multiple conformations of the spin-label, an issue of critical relevance to the structural interpretation of the distances. The distances and distributions found in this study are readily rationalized in terms of the known crystal structure, the characteristic conformers of the nitroxide side chains, and molecular modeling. This study sets the stage for the use of DQC-ESR for determining the tertiary structure of large proteins with just a small number of long-distance constraints.

Introduction

The process of protein structure determination by spectroscopic methods relies primarily on the measurement of distances on a scale that is relevant to the macromolecular structure. These distances serve as constraints in computational procedures to reduce the number of degrees of freedom available to the polypeptide chain, to orient and dock proteins that participate in supramolecular assemblies, and to characterize the time evolution of these structures during their function. The efforts to develop approaches for distance measurements are particularly timely in the context of structural genomics for problems that are currently not amenable to study by X-ray crystallography. Notable examples include the static structure of membrane proteins and conformationally heterogeneous water-soluble proteins and the equilibrium fluctuations in these structures or their induced conformational changes. In this context, ESR spectroscopy in combination with site-directed spin-labeling[1] (SDSL) provide a window with unique capabilities onto these issues.[2] SDSL is based on the insertion of nitroxide spin-labels at natural or mutagenically introduced cysteine residues, as illustrated in Figure 1, for a methanethiosulfonate nitroxide reagent, which produces the side chain referred to as R1.

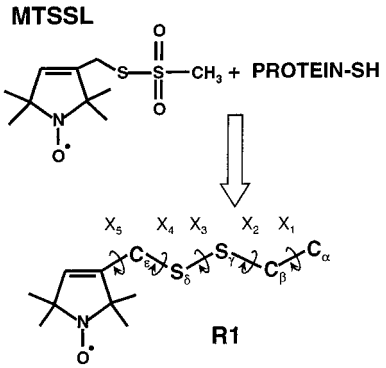

Figure 1. Protein labeling with MTSSL spin-label used in this work. After labeling, the nitroxide moiety is tethered to the backbone via a side chain referred to as R1. Note that the C_α and C_β carbons are on the cysteine residue with the C_α position in the backbone. The dihedral angles X1−X5 are also shown (cf. ref 60).

The most extensive use of distances for structure determination has been in the context of NMR spectroscopy. The geometric information is usually derived from NOE-based experiments in the form of a distance with upper and lower bounds. The number of such constraints required for the determination of a structure of biologically relevant resolution depends on the range and quality of such constraints. In general, fewer longer-range (as compared to short-range) distances are

* To whom correspondence should be addressed. E-mail: jhf@ccmr.cornell.edu.
[†] Cornell University.
[‡] Vanderbilt University School of Medicine.

(1) Hubbell, W. L.; Altenbach, C. *Curr. Opin. Struct. Biol.* **1994**, *4*, 566.
(2) Berliner, L. J., Eaton, G. R., Eaton, S. S., Eds. *Biological Magnetic Resonance: Distance Measurements in Biological Systems by EPR*; Kluwer Academic: New York, 2000; Vol. 19.

10.1021/ja020040y CCC: $22.00

needed. Thus, considerable efforts have been directed to develop NMR methods capable of measuring longer distances.

These considerations are even more important in reporter group techniques where the measurements of distances require the choice and preparation of sites where the probes are to be attached. Thus, in addition to resolution, range and quality are determinants of experimental throughput. In ESR spectroscopy, where the reporter is a nitroxide spin-label, current strategies for distance measurements rely primarily on cw-ESR of doubly labeled proteins. In cw-ESR, one must determine the added (often weak) effect of the intramolecular dipolar interaction between the two spin-labels on the nitroxide powder spectra, which is usually dominated by the nitrogen hyperfine (hf), g-tensors, and unresolved proton couplings. This requires comparison with the spectra from singly labeled species. For distances shorter than 15 Å, the dipolar coupling becomes comparable to the other sources of inhomogeneous broadening of the nitroxide spectra. In this case, the dipolar broadening can be reliably extracted from cw-ESR spectra. The case of relatively strong dipolar coupling has been extensively studied by cw-ESR,[3−15] with quantitative analysis in several cases.[3−11,15] This, in turn, has allowed for the discrimination between possible configurations of protein subunits. In key studies, it was possible to quantify distances of up to ca. 20 Å using single-label referencing[7−11] and even to determine mutual orientations of nitroxides in some cases.[5,6]

Pulsed ESR methods comprise a powerful set of tools for measuring distances over a broad range, from 15 Å to at least 50 Å, for obtaining distance distributions, for analyses of structural correlations, and for spin-counting.[16−35] These methods were developed largely to overcome the limitations and weaknesses of cw-ESR. They are based on the detection of spin−echoes where the dominant effects of the hf and g-tensors cancel, leaving just the dipolar interaction. In addition, in pulsed methods the contributions to the signals from the doubly labeled molecules usually are distinct from those from singly labeled ones, and thus the latter can be removed without the need for single-label referencing,[19,32] as we also illustrate in this work.

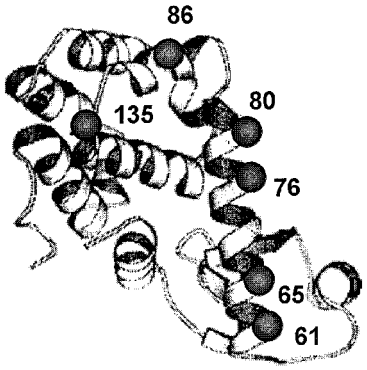

Figure 2. Ribbon structure of T4L, showing spin-labeled mutated sites studied in this work.

In this study, a novel pulsed ESR method, double-quantum coherence (DQC) ESR spectroscopy,[26,33−35] has been applied to a protein of known structure, T4L, shown in Figure 2, along with the labeling sites used in this study. Its advantages over previous pulsed methods include higher intrinsic sensitivity, since (nearly) all the spins may be irradiated; the suppression of complicating features due to correlations between orientations of the magnetic tensors of the nitroxide and the inter-radical vector; and the filtering of undesirable artifacts.[34,35]

Our results demonstrate the feasibility of measuring distances in spin-labeled proteins of at least up to 50 Å. In this range, the relative importance of the linking arm, conformational preferences, and local interactions of the nitroxide on the structural interpretation of these distances is reduced. Our initial analysis of the distance distribution does, however, reveal their importance in aiding the interpretation of these distances.

DQC and Distance Measurements

The spin Hamiltonian for a pair of nitroxides at high field in the point dipole approximation can be written in the form:

$$H/\hbar = (\beta/\hbar)\mathbf{B}\cdot\mathbf{g}_1\cdot S_{1z} + \mathbf{I}_1\cdot\mathbf{A}_1\cdot S_{1z} + (\beta/\hbar)\mathbf{B}\cdot\mathbf{g}_2\cdot S_{2z} + \mathbf{I}_2\cdot\mathbf{A}_2\cdot S_{2z} + D(3\cos^2\theta - 1)\left(S_{1z}S_{2z} - \frac{\mathbf{S}_1\cdot\mathbf{S}_2}{3}\right) + J\left(\frac{1}{2} - 2\mathbf{S}_1\cdot\mathbf{S}_2\right) \quad (1)$$

(3) Farhbakhsh, Z. T.; Huang, Q. L.; Ding, L. L.; Altenbach, C.; Steinhoff, H. J.; Horwitz, J.; Hubbell, W. L. *Biochemistry* **1995**, *34*, 509.
(4) Hanson, P.; Millhauser, G.; Formaggio, F.; Crisma, M.; Toniolo, C. *J. Am. Chem. Soc.* **1996**, *118*, 7618.
(5) Hanson, P.; Anderson, D. J.; Martinez, G.; Millhauser, G.; Formaggio, F.; Crisma, M.; Toniolo, C.; Vita, C. *Mol. Phys.* **1999**, *95*, 957.
(6) Hustedt, E. J.; Smirnov, A. I.; Laub, C. F.; Beth, A. H. *Biophys. J.* **1997**, *72*, 1861.
(7) Rabenstein, M. D.; Shin, Y. K. *Proc. Natl. Acad. Sci. U.S.A.* **1995**, *92*, 8239.
(8) Rabenstein, M. D.; Shin, Y. K. *Biochemistry* **1996**, *35*, 13922.
(9) Xiao, W. Z.; Poirier, M. A.; Bennett, M. K.; Shin, Y. K. *Nat. Struct. Biol.* **2001**, *8*, 308.
(10) Xiao, W. Z.; Brown, L. S.; Needleman, R.; Lanyi, J. K.; Shin, Y. K. *J. Mol. Biol.* **2001**, *304*, 715.
(11) Altenbach, C.; Oh, K. J.; Trabanino, R. J.; Hideg, K. H.; Hubbell, W. L. *Biochemistry* **2001**, *40*, 15471.
(12) Mchaourab, H. S.; Oh, K. J.; Fang, C. J.; Hubbell, W. L. *Biochemistry* **1997**, *36*, 307.
(13) Hubbell, W. L.; Cafiso, D. S.; Altenbach, C. *Nat. Struct. Biol.* **2000**, *7*, 735.
(14) Koteiche, H. A.; Mchaourab, H. S. *J. Mol. Biol.* **1999**, *294*, 561.
(15) McNulty, J. C.; Silapie, J. L.; Carnevali, M.; Farrar, C. T.; Griffin, R. G.; Formaggio, F.; Crisma, M.; Toniolo, C.; Milhauser, G. L. *Biopolymers* **2000**, *55*, 479.
(16) Borbat, P. P.; Berdnikov, V. M.; Milov, A. D.; Tsvetkov, Y. D. *Sov. Phys. Solid State* **1977**, *19*, 628.
(17) Milov, A. D.; Salikhov, K. M.; Shirov, M. D. *Sov. Phys. Solid State* **1981**, *23*, 565.
(18) Milov, A. D.; Maryasov, A. G.; Tsvetkov, Y. D. *Appl. Magn. Reson.* **1998**, *15*, 107.
(19) Milov, A. D.; Maryasov, A. G.; Tsvetkov, Y. D.; Raap, J. *Chem. Phys. Lett.* **1999**, *303*, 135.
(20) Milov, A. D.; Tsvetkov, Y. D.; Formaggio, F.; Crisma, M.; Toniolo, C.; Raap, J. *J. Am. Chem. Soc.* **2001**, *123*, 3784.
(21) Ichikawa, T.; Wakasugi, S. I.; Yoshida, H. *J. Phys. Chem.* **1985**, *89*, 3583.
(22) Raitsimring, A. M.; Salikhov, K. M. *Bull. Magn. Reson.* **1985**, *7*, 184.
(23) Kurshev, V. V.; Raitsimring, A. M.; Tsvetkov, Y. D. *J. Magn. Reson.* **1989**, *81*, 441.
(24) Larsen, R. G.; Singel, D. J. *J. Chem. Phys.* **1993**, *98*, 5134.
(25) Saxena, S.; Freed, J. H. *J. Chem. Phys.* **1997**, *107*, 1317.
(26) Borbat, P. P.; Costa-Filho, A. J.; Earle, K. A.; Moscicki, J. K.; Freed, J. H. *Science* **2001**, *291*, 266.
(27) Pannier, M.; Veit, S.; Godt, A.; Jeshke, G.; Spiess, H. W. *J. Magn. Reson.* **2000**, *142*, 331.
(28) Jeschke, G.; Pannier, M.; Godt, A.; Spiess, H. W. *Chem. Phys. Lett.* **2000**, *331*, 243.
(29) Dzuba, S. A.; Bosh, M. K.; Hoff, A. J. *Chem. Phys. Lett.* **1996**, *248*, 427.
(30) Dzuba, S. A.; Kawamori, A. *Concepts Magn. Reson.* **1996**, *8*, 49.
(31) Dzuba, S. A.; Hoff, A. J. In *Biological Magnetic Resonance: Distance Measurements in Biological Systems by EPR*; Berliner, L. J., Eaton, G. R., Eaton, S. S., Eds.; Kluwer Academic: New York, 2000; Vol. 19, p 569.
(32) Raitsimring, A.; Peisach, J.; Lee, H. C.; Chen, X. *J. Phys. Chem.* **1992**, *96*, 3526.
(33) Saxena, S.; Freed, J. H. *Chem. Phys. Lett.* **1996**, *251*, 102.
(34) Borbat, P. P.; Freed, J. H. *Chem. Phys. Lett.* **1999**, *313*, 145.
(35) Borbat, P. P.; Freed, J. H. In *Biological Magnetic Resonance: Distance Measurements in Biological Systems by EPR*; Berliner, L. J., Eaton, G. R., Eaton, S. S., Eds.; Kluwer Academic: New York, 2000; Vol. 19, p 383.

Here, $\mathbf{g}_1$, $\mathbf{g}_2$ are the g-tensors, and $\mathbf{A}_1$, $\mathbf{A}_2$ are the hf tensors of the nitroxides, labeled 1 and 2, $D = 3\gamma_e^2\hbar/2r^3$ is the dipolar spin−spin interaction constant, and J is the electron exchange integral. The nonsecular terms have been dropped, as is appropriate at high magnetic fields. Nuclear Zeeman and quadrupolar interactions have been omitted, as is suitable at X (9 GHz)- or Ku (17 GHz)-band for the ^{14}N nucleus of the nitroxide.[18,22,25] For nitroxide labels separated by 15 Å or more, the electron exchange can usually be ignored. Weak hf interactions with other nuclei have also been ignored. They can still lead to electron spin−echo envelope modulation[36,37] (ESEEM), as outlined elsewhere,[35] and their effects will be discussed later. We assume the rigid limit, with relaxation effects dealt with as needed. The rigorous treatment of relaxation for nitroxides and for dipolar-coupled systems has been developed.[38−43] The Hamiltonian of eq 1 can be written in the form:

$$H/\hbar = \Omega_1 S_{1z} + \Omega_2 S_{2z} + aS_{1z}S_{2z} - a(S_1^+ S_2^- + S_1^- S_2^+)/4 \quad (2)$$

where

$$a = 2D(1 - 3\cos^2\theta)/3 \quad (3)$$

Here Ω_1 and Ω_2 represent the Larmor frequencies of the coupled electron spins 1 and 2 due to their hf and g-tensors and their mutual orientations, the details of which can be found elsewhere.[25,38] The Hamiltonian in the form of eq 2 is sufficient to describe the DQC experiment.[35]

The distances between dipolar coupled electron spins enter via the constant of dipolar interaction, D. It is the long-range property of this interaction that makes it possible to measure distances of up to ca. 20 Å by cw-ESR and to about 60−80 Å by pulsed ESR techniques.[2,35]

A rigorous numerical treatment of DQC-ESR for the nitroxide biradicals using the Hamiltonian of eq 1 was first developed by Saxena and Freed.[25] An approximate approach,[34] which allows one to obtain closed-form solutions by product operator techniques,[44,45] is suitable for pulsed methods when the dipolar coupling is weak as compared to the anisotropic parts of the Zeeman and hf tensors. Qualitatively, this assumption is equivalent to the absence of significant visible dipolar broadening in cw-ESR spectra. In this case, the pseudosecular or flip-flop terms (i.e., terms in $S_1^{\pm}S_2^{\mp}$) of the dipolar part of the spin Hamiltonian, given by eq 2, can be omitted. The only remaining complication in this case is the effect of spatial correlations between magnetic tensors of coupled nitroxides.[24,25,46,47] However, these correlations can be either suppressed in the DQC experiment by using large microwave magnetic fields, B_1's, or studied by a 2D-FT DQC technique.[35]

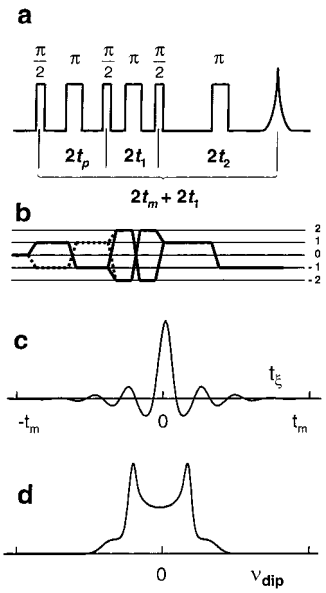

Figure 3. The six-pulse DQC sequence (a) is shown with the corresponding coherence pathways (b). In this sequence the sum, $t_m \equiv t_p + t_2$, is kept constant (t_1 is also set constant). The echo amplitude is recorded vs $t_\xi \equiv t_p - t_2$ (c), and it is symmetrical with respect to $t_\xi = 0$. Cosine Fourier transformation of (c) produces the dipolar spectrum (d).

A more general solution for DQC using eq 2 (i.e., including terms in $S_1^{\pm}S_2^{\mp}$) is possible when the dipole−dipole coupling is much smaller than B_1. In this case, it was possible to obtain closed-form expressions for the DQC signal, using a modified product operator method.[35] In this limit, the effect of the dipole−dipole coupling during the intense pulses is small. Its neglect is the only approximation that is made. The signal in this treatment can be represented as a product of second rank matrixes. It is then possible to arrive at manageable algebraic expressions[35] [which also provide detailed insight into the mechanisms of all the known pulse sequences of ESR dipolar spectroscopy[17,23,28]].

In applications of the DQC method, the six-pulse sequence, shown in Figure 3, has been most useful. In this sequence, the evolution of electron spin coherences due to the dipolar interaction is selectively detected. The temporal envelope of the DQ signal is Fourier transformed, to yield the dipolar spectrum as shown in the same figure. The dipolar spectrum of a biradical assumes the shape of a Pake pattern[48] with a splitting of $4D/3$ between the turning point peaks in the typical case for pulsed ESR of weak coupling, which corresponds to distances exceeding ca. 20 Å.[24,34,46]

This sequence has been tested at Ku-band, using rigid organic biradicals and synthetic peptides.[34,35] There it was demonstrated that it yields Pake doublets, by the use of biradicals with 16 and 29 Å distances between electron spins. The signal-to-noise ratio was good even though T_2's were in the range of 0.35−0.8 μs at a temperature of ca. 204 K. An improvement of S/N is a distinct feature of coherent pulsed methods, where a large portion (or all) of the ESR spectrum can be excited.

In the limit of full excitation, the DQC dipolar signal takes on a particularly simple form: $-\sin at_p \sin a(t_m - t_p) = {}^1/_2[\cos$

(36) Kevan, L. In *Time-Domain Electron Spin Resonance*; Kevan, L., Bowman, M. K., Eds.; Wiley: New York, 1979; Chapter 8.
(37) Dikanov, S. A.; Tsvetkov, Y. D. *Electron Spin−Echo Envelope Modulation (ESEEM) Spectroscopy*; CRC Press: Boca Raton, FL, 1992; p 21.
(38) Lee, S.; Patyal, B. R.; Freed, J. H. *J. Chem. Phys.* **1993**, *98*, 3665.
(39) Lee, S.; Budil, D. E.; Freed, J. H. *J. Chem. Phys.* **1994**, *101*, 5529.
(40) Nevzorov, A. A.; Freed, J. H. *J. Chem. Phys.* **2000**, *112*, 1425.
(41) Nevzorov, A. A.; Freed, J. H. *J. Chem. Phys.* **2000**, *112*, 1413.
(42) Nevzorov, A. A.; Freed, J. H. *J. Chem. Phys.* **2001**, *115*, 2401.
(43) Nevzorov, A. A.; Freed, J. H. *J. Chem. Phys.* **2001**, *115*, 2416.
(44) Sørensen, O. W.; Eich, G. W.; Levitt, M. H.; Bodenhausen, G.; Ernst, R. R. *Prog. Nucl. Magn. Reson. Spectrosc.* **1983**, *16*, 163.
(45) Slichter, C. P. *Principles of Magnetic Resonance*; Springer-Verlag: Berlin−Heidelberg−New York, 1990.
(46) Maryasov, A. G.; Tsvetkov, Y. D.; Raap, J. *Appl. Magn. Reson.* **1998**, *14*, 101.
(47) Hustedt, E. J.; Beth, A. H. *Annu. Rev. Biophys. Biomol. Struct.* **1999**, *28*, 129.
(48) Pake, G. E. *J. Chem. Phys.* **1948**, *16*, 327.

$at_m - \cos at_\xi$], where $t_\xi \equiv t_p - t_2$ (cf. Figure 3c). Yet we shall use the full theory of Borbat and Freed,[34,35] which necessarily includes averaging "*a*" over all orientations (cf. Figure 3).

The noticeable advantage of this six-pulse sequence is that it filters out coherence pathways which are not created by the dipolar interactions. It is effectively dead-time free, since the echo is always detected at the same time $2t_m + 2t_1$ (cf. Figure 3a), even though t_2 and t_p are varied. Note that each step in the coherence pathway (cf. Figure 3b) precisely refocuses the hf and g-tensor inhomogeneities and that one collects the echo envelope as a function of $t_\xi = t_p - t_2$ (cf. Figure 3c). The dipolar coupling is itself partially refocused at $t_\xi = 0$, when $t_p = t_2$, yielding a symmetric signal with respect to t_ξ.

The six-pulse DQ sequence does sense the DQC formed by the dipole−dipole interactions with other electron spins in the sample. These intermolecular interactions produce an effect on the signal that appears as a small baseline, which is close to linear in t_ξ (except at very high concentrations), and it is also symmetrical with respect to $t_\xi = 0$, that is, refocused at $t_\xi = 0$. Usually, this baseline in the DQC signal envelope can readily be removed, as we illustrate below. We will call all other unrefocused effects from the dipole−dipole interactions as instantaneous diffusion,[49,50] which therefore includes effects of development of higher orders of coherence among all the spins in the sample as described by Nevzorov and Freed.[42] We show below that it is insignificant for the experimental conditions of this work. Also, we show how we conveniently remove the residual effect of nuclear spin diffusion, which becomes the dominant relaxation process at very low temperatures.[43,51−53]

Experimental Section

Mutants T4L, 61/135, 65/135, 135/80, 61/86, 65/86, 61/80, 65/80, 65/76 were constructed as previously described.[54] The proteins were expressed in the *Escherichia coli* K38 and the proteins purified by cation exchange chromatography following the protocol of Mchaourab et al.[54] Excess spin-label MTSSL (cf. Figure 1) was added and incubated for 2 h at room temperature. Unreacted spin-label was removed by desalting, and the samples were concentrated and further washed in three dilution/concentration cycles. Aqueous solutions of T4L in concentrations of ca. 0.5−1 mM were buffered with 20 mM MOPS, 100 mM NaCl, 0.1 mM EDTA, and 0.02% sodium azide for pH 7.2. Thirty weight % sucrose was added as a cryoprotectant. Some of the T4L solutions were also prepared by adding wild-type T4L in molar ratios of 1:2 for 80/135 and 1:1 for 65/80 to check whether there was phase separation in the frozen solutions.

All studies were performed using a home-built X/Ku-band 2D-FT-ESR spectrometer[55] at working frequencies of 9.2 and 17.35 GHz, respectively. Whereas Ku-band has some advantages, noted below, currently the Ku-band setup is optimized for studies of molecular dynamics, so the achievable sample temperature, provided by nitrogen gas flow, was limited to >150 K. For this reason, Ku-band was used mainly in the early stages of this work for the mutants with <25 Å distance between spin-labels since this frequency provides better resolution than does X-band for shorter distances.[35] Ku-band was not used for measurements of long distances, due to the rather short nitroxide T_2's of ca. 300−350 ns at the local T_2 maximum occurring at about 200 K. At Ku-band, $\pi/2$ pulses were about 3.2 ns corresponding to a B_1 of ca. 30 G.[34] For distances exceeding 25 Å, requiring longer T_2's, the experiments were conducted at 77 K at X-band (9.2 GHz) using a standard TE_{012} rectangular cavity resonator and a liquid nitrogen fingertip Dewar flask. At this temperature, the T_2's (more precisely the phase memory times T_m) were ca. 4 μs. This permits a longer t_ξ, which is required to observe the slower dipolar oscillations for the longer distances. In this 9.2 GHz resonator, it was only possible to realize $\pi/2$ pulses of 8 ns, corresponding to a B_1 of ca. 11 G, using the full power available from the TWTA (model 174X/Ku, Applied System Engineering). This was acceptable for distances exceeding 30 Å, although it did not result in optimal sensitivity. The resonator Q's were in both cases reduced sufficiently that the bandwidth of the experiment was determined by the respective B_1's (this corresponded to loaded Q's of about 75 at Ku-band and about 120 at X-band).

For measurements at Ku-band, 10−15 μL volumes of solutions of doubly spin-labeled T4L mutants 65/76, 61/80, and 65/80 were placed into 2 mm i.d. quartz sample tubes and sealed. For X-band measurements, the solutions containing doubly labeled mutants 61/135, 65/135, 80/135, 61/86, 65/86, 61/80, 65/80 were sealed in standard 4 mm o.d. ESR quartz sample tubes in ca. 80 μL amounts. Some of the samples (80/135, 65/86, 61/135, 65/135) were further diluted with buffer, containing 60 wt % sucrose, by a factor of 2−3 to final concentrations of ca. 0.25−0.35 mM. Samples with sucrose concentrations in excess of ca. 50 wt % formed transparent glasses upon freezing in liquid nitrogen. The samples more diluted in sucrose had a snowlike appearance. However, we have not detected effects indicating that the protein was driven out into a separate phase (cf. below).

Most of the results were obtained using the six-pulse DQC sequence, as described above. At Ku-band, the pulse repetition rate was 10 kHz, whereas at X-band it was typically set to 1−2.5 kHz due to longer T_1's at the lower temperature. T_m's were obtained using primary echo (PE) sequences ($\pi/2-\pi/2$ or $\pi/2-\pi$), with a $\pi/2$ pulse of width 3.2 ns at Ku-band and from 10 to 40 ns at X-band. Good DQC signals were typically obtained after about 40 min of signal averaging, although up to 2 h of averaging was employed for the larger distance cases.

Data Analysis. In DQC-ESR, as we have shown,[35] the dipole−dipole modulation is detected virtually undistorted. With just minor corrections (referred to above), prior to Fourier transformation, a very clean dipolar spectrum is obtained. The intermolecular DQC signal has already been briefly discussed. Other effects originate from the phase relaxation of the electron spins, that we consider now.

The six-pulse DQC sequence cancels basic relaxation processes which decay exponentially as noted above, so no correction is required for them. However, at low temperatures (77 K), phase relaxation is largely determined by nuclear spin diffusion of the matrix protons, which modulate their many-body dipolar interactions with the electron spin, yielding a T_m for the primary echo of 4−10 μs at typical proton concentrations of the solvents used.[51,52] In particular, Lindgren et al.[52] found a T_m for spin-labeled proteins in water−glycerol solutions in the range of 4−4.4 μs at low temperatures with a power law of 2 ± 0.1 for labels in contact with the aqueous phase. We have studied the X-band PE decays at 77 K, and we also find a power law of 2 ± 0.1 with T_m's in the range of 4−4.4 μs. This is expected, since in our study the spin-labels were located on the protein surfaces in good contact with the aqueous phase. Thus, we conclude that at 77 K the dominant phase relaxation is due to proton spin diffusion.

A quadratic decay law is not fully canceled by the "zero dead-time" six-pulse DQC sequence of Figure 3. The signal decay, which occurs during each of the varying time intervals $2t_p$ and $2(t_m - t_p)$, corresponding to ± 1 order of coherence, results in a variation of the signal envelope recorded as a function of $t_\xi \equiv 2t_p - t_m$. Rewriting these intervals as $t_m \pm t_\xi$, the decay $V_R(t_\xi, t_m)$ in the six-pulse sequence by

(49) Klauder, J. R.; Anderson, P. W. *Phys. Rev.* **1962**, *125*, 913.
(50) Raitsimring, A. M.; Salikhov, K. M.; Umanskii, B. A.; Tsvetkov, Y. D. *Sov. Phys. Solid State* **1974**, *16*, 492.
(51) Milov, A. D.; Salikhov, K. M.; Tsvetkov, Y. D. *Sov. Phys. Solid State* **1973**, *15*, 802.
(52) Zecevic, A.; Eaton, G. R.; Eaton, S. S.; Lindgren, M. *Mol. Phys.* **1998**, *95*, 1225.
(53) Lindgren, M.; Eaton, G. R.; Eaton, S. S.; Johnsson, B. H.; Hamarström, P.; Svensson, M.; Carlsson, U. *J. Chem. Soc., Perkin Trans.* **1997**, *2*, 2549.
(54) Mchaourab, H. S.; Lietzow, M. L.; Hideg, K.; Hubbell, W. L. *Biochemistry* **1996**, *35*, 7692.
(55) Borbat, P. P.; Crepeau, R. H.; Freed, J. H. *J. Magn. Reson.* **1997**, *127*, 155.

this mechanism for like radicals is

$$V_R(t_m,t_\xi) = e^{-(t_m + t_\xi/T_m)^2 - (t_m - t_\xi/T_m)^2} = e^{-(1/2)(2t_\xi/T_m)^2 - (1/2)(2t_m/T_m)^2} \propto [e^{-(2t_\xi/T_m)^2}]^{1/2} \quad (4)$$

Thus, for a quadratic law there is a signal decay versus t_ξ that is much slower than that for the primary echo, that is, by its square root. This is expected in pulse sequences with multiple refocusing, which suppress spectral diffusion.[56]

Thus, we could extract the magnitude of T_m from the faster primary echo decay and then use this result to correct the DQC signal according to eq 4. Actually, this correction does not need to be very accurate, since it just serves to reduce the relaxation broadening, thereby improving the fit in the time domain. (In fact, standard data apodization by applying a window prior to Fourier transforming would have an even stronger effect on the signal than would an uncompensated decay.) For very long distances, this correction does become more significant. However, in that case, the main problem is the limited time scale over which the signal is detected (equivalent to the apodizing effect). The corrections were made according to eq 4 by multiplying the signal with $\exp[2(t_\xi/T_m)^2]$. We found that 10% accuracy in T_m is sufficient. For our experiments, the correction was a factor of 2.4 at the endpoints (i.e., $t_\xi = \pm t_m$) for the largest t_m values used.

In the case of the higher temperatures (204 K) used for Ku-band, spin diffusion was not significant. The PE decayed by a simple exponential law, which is readily canceled out in the zero dead-time experiment.

The next task is to separate the inter- and intramolecular contributions to the signal. Our experiments were performed at low enough concentrations that the latter were small. The analysis and study of intermolecular effects for DQC[34,35] lead to simple exponential decay in $|t_\xi|$ proportional to the concentration. The fact that it is weak in our experiments over time intervals of order t_m meant that it could readily be fit with a functional form: $S_{inter}(t_\xi) \approx b(t_m - |t_\xi|)$.

The procedure for signal processing in the time domain is illustrated in Figure 4 for the 65/86 mutant. After making the correction for the quadratic decay, the intramolecular signal is simulated with seed parameters, scaled, and then subtracted from the experimental data. When the residual baseline is close to the expected linear profile about t_ξ, the latter is approximated by a second-degree polynomial and then subtracted from the signal data. The remainder is then Fourier transformed and compared with the Fourier transformation of the simulated time-domain signal to refine simulation parameters. (The comparisons are also made in the time domain.) This self-consistent procedure is repeated two to three times before the baseline reaches its final shape.

In cw-ESR studies of dipolar coupling, a careful analysis of the results requires that one consider the orientational correlations between the magnetic tensors of the nitroxide and the interradical vector.[47] However, in most studies (including pulse-ESR methods), consideration of this has been avoided, and instead it was assumed that the nitroxides are uncorrelated.[2,7−14,18−20,27−29,32,34] This correlation is also an important issue in a rigorous analysis of pulse-ESR methods based on partial irradiation, such as double electron−electron resonance (DEER, also known as PELDOR).[19,24] A major virtue of DQC-ESR is that one can suppress the complicating features of such correlations by the use of very strong pulses. Our use of strong 30 G B_1 pulses at Ku-band is consistent with suppression (although not complete removal) of such complications. At X-band, the static field was set to excite the $m_I = 0$ spectral region of the ^{14}N spectrum with 11 G B_1 pulses, also reducing these effects. For convenience, we have therefore assumed the uncorrelated case in our simulations. There is some additional justification for this, which we discuss below in the section on distance distributions.

(56) Carr, H. Y.; Purcell, E. M. *Phys. Rev.* **1954**, *94*, 630.

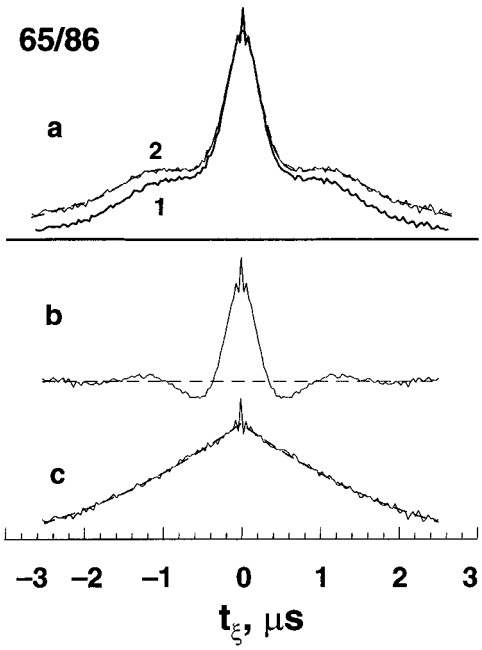

Figure 4. DQC signal refinement: X-band and 77 K. (Curves a, b, and c are on the same scale). (a) DQC signal envelope from the six-pulse DQC sequence for the 65/86 mutant before (1) and after (2) correction for the decay, caused by phase relaxation due to nuclear spin diffusion. Dashed line in (2) is a fit to the experimental data that are a sum of the intramolecular (panel b) and intermolecular (panel c) signals. (b) The intramolecular DQC signal obtained after subtraction of the fit to the baseline (the dashed line in panel c). (c) The intermolecular DQC signal (solid line) isolated by the subtraction of the simulated intramolecular signal from the full signal [panel a, (2)].

Another virtue of DQC-ESR over cw-ESR is that incomplete labeling can be of some concern in the latter[7−10] but not in the former.[35] If there are singly labeled proteins in the sample they will not contribute at all to the relevant intramolecular part of the DQC-ESR signal. Of course, they contribute to the weak baseline due to intermolecular broadening that is removed by the procedure discussed above.

Another effect is ESEEM due to surrounding protons. ESEEM interferes to varying extents with all of the techniques based on pulse sequences using a single frequency, but can be suppressed at sufficiently high frequencies. ESEEM was observed in DEER as well.[27] In DQC, ESEEM has just a small effect at Ku-band, but at X-band it is more significant. There are a number of ways to suppress nuclear modulation. They are based on using "blind spots"[27,34] as well as on integration of the signal versus one of the independent time variables.[28,57] To minimize nuclear modulation, we summed four data collections, with t_m being stepped out by a half period of the nuclear Zeeman frequency. For long distances and at Ku-band, the effect on the signal was largely cosmetic, so that usually ESEEM effects can be ignored or avoided. At X-band, especially at shorter distances, modulation at the nuclear Zeeman frequency, ν_I, which enters in six-pulse experiments as $\nu_I/2$ (i.e., ca. 7 MHz for protons at X-band), does interfere with the dipolar spectrum.[58] By using the procedure described, the effect was suppressed nearly completely.

Results and Discussion

Distances. Representative results from DQC on several doubly labeled T4L mutants covering the distance range from about 20 Å to about 50 Å are shown in Figures 5 and 6 along

(57) Astashkin, A. V.; Raitsimring, A. M. *J. Magn. Reson.* **2000**, *143*, 280.
(58) Nuclear modulation also depends on t_1, which was typically set at about 70 ns at X-band, where the signal passes through a nuclear modulation maximum.

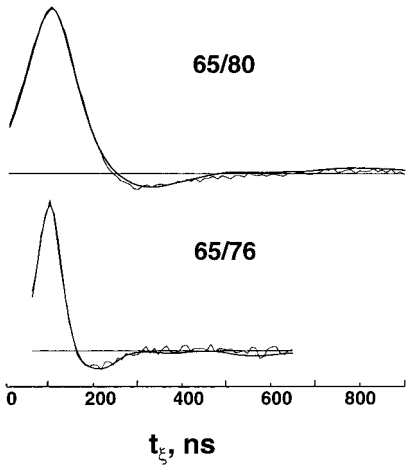

Figure 5. Results from the six-pulse DQC sequence for two T4L mutants obtained at 17.3 GHz, 204 K using a B_1 of 30 G. At this temperature no correction for phase relaxation due to nuclear spin diffusion was required. The fits to the data using model 1 from Figure 10 are plotted in solid lines.

with their fits.[59] The distances were extracted by fitting the spectra as already described. The dipolar spectra produced by Fourier transforming the signal envelopes after data processing are shown for three representative mutants in Figure 6. However, in our data fitting we consistently found that the spectra were broader than one would expect for a rigid structure, but amenable to fitting using distributions in distances. This is also clear from the time-domain spectra wherein the oscillations of the signals versus t_ξ, expected for well-defined distances,[34,35] decay more rapidly, and in some cases are difficult to observe. In general, there are several sources of broadening: (i) the distribution of conformations in T4L; (ii) the flexibility of the tether of the spin-label used in this study; (iii) limited spectral resolution due to the finite length of the sampling interval constrained by the phase relaxation; and (iv) broadening caused by flip-flop terms of the dipolar coupling (cf. eq 2). Experiments with rigid biradicals at Ku-band[34,35] indicated that for distances exceeding 25 Å source, (iv) could be ruled out. For weaker pulses at X-band, such effects could be more pronounced. However, by numerical simulations, we confirmed that for distances exceeding 30 Å, the effect of (iv) was definitely too weak to account for the observed extent of spectral broadening (cf. Figure 6 and below). The source (iii) limits spectral resolution by ca. 0.15 MHz for the sampling interval we used of ca. 3 μs, which is insignificant for distances below 40 Å. It cannot account for the observed spectral broadening. Therefore, the first two should be the primary broadening sources.

We summarize the results for all the mutants in Tables 1 and 2, where the distances are listed together with the parameters connected with distribution widths. Because of significant distribution widths and finite spectral resolution, the distances were determined to an accuracy of ca. $\pm 1.5-2$ Å with the larger uncertainty for longer distances. The distance distributions will be detailed later in this section. The simulated dipolar spectra are shown in Figure 6 for comparison with experimental spectra. For the mutants labeled at site 61, the distributions were consistently found to be bimodal at 77 K, indicating the presence of two sites or conformers at this position weighted in a 1:2 ratio (cf. Figure 9).

At Ku-band, the dipolar spectra were slightly broader than those at X-band, as we observed for the 65/80 mutant. This can be explained either by residual motion of the labeled protein and/or by a wider distribution of the labeled protein conformers at the temperature of 204 K for the Ku-band experiments. There is also some difference in the distances obtained at the two working frequencies (and respective temperatures). Although it is of the level of the experimental uncertainty, it might be explained by spin-label and/or protein conformers at 204 K favoring decreased distances. Similar effects were seen for 61/80, which, however, is complicated by the bimodal distribution seen at 77 K. The Ku-band results for this mutant had sufficiently reduced S/N that we refrained from including the results in Table 1. However, the overall width and shape of the distribution are similar to that at X-band and 77 K. The 65/76 mutant represents the shortest distance (21.4 Å) we studied, and the only one (barely) amenable to cw methods. We note good agreement with the recent cw-ESR results for this mutant.[11] Given the sharper and better resolved dipolar spectra for X-band and 77 K, we use these results in Table 2 in the further analyses below.

Addition of unlabeled wild-type T4L to solutions of 80/135 and 65/80 caused only a minor change in the signal amplitudes and envelopes, slightly narrowing the distributions for 80/135. The dilution of 65/135, 61/135, and 80/135 by buffer containing 60 wt % sucrose did not produce a noticeable effect on the (processed) dipolar spectral shapes of these mutants. Also, the signal amplitude varied nearly linearly with concentration. All of this indicates a low level of aggregation and phase separation effects as well as an insignificant role of instantaneous diffusion in this work.

In Figure 7, the distances between different mutated sites are shown to form 3-D structures. The volumes representing the range of space occupied by the nitroxide NO groups are depicted as light gray spheres with an average radius reflecting the typical distributions (as found from fitting of the DQC decay, cf. Tables 1 and 2, and below). It is clear that, relative to these long distances, the volume available for the nitroxides is small enough to result in an accurate 3-D model. The dark sphere indicates an additional spin-labeled site, which would be needed to obtain the distances, drawn in dashed lines, with the goal of completing the tetrahedra to map the protein (including the spin-labeled side chains) onto a rigid frame. (For the 86 mutant, our limited measurements are insufficient to fix its position with respect to the mutated sites shown in the figure. Also, the distance between 80 and 86 is too short to be determined accurately, so other double mutants would be desirable to reconstruct the 3-D model of the nitroxide positions.)

Molecular Modeling. The distances, R_{av}, reported in Table 2 (as well as Table 1) reflect the separation between the nitroxide moieties tethered by the R1 side chains to the backbone (cf. Figure 1, which shows five bonds connecting the C_α on the backbone to the nitroxide ring). There is as yet no established approach to relate these distances to those between the corresponding C_α's (i.e., $R_{\alpha\alpha}$). The main uncertainty arises from the flexibility of the linking arm (i.e., the side chain not including the nitroxide ring) and the tendency of the R1 side chain to participate in local interactions. For the present study, we

(59) At 77 K (X-band), t_ξ was varied over the whole range from $\pm t_m$ as shown in Figures 4 and 6 to provide spectra symmetric in t_ξ. At 200 K (Ku-band), with shorter t_m we found we could optimize data acquisition (hence S/N) by collection of just $t_\xi \geq 0$, cf. Figure 5.

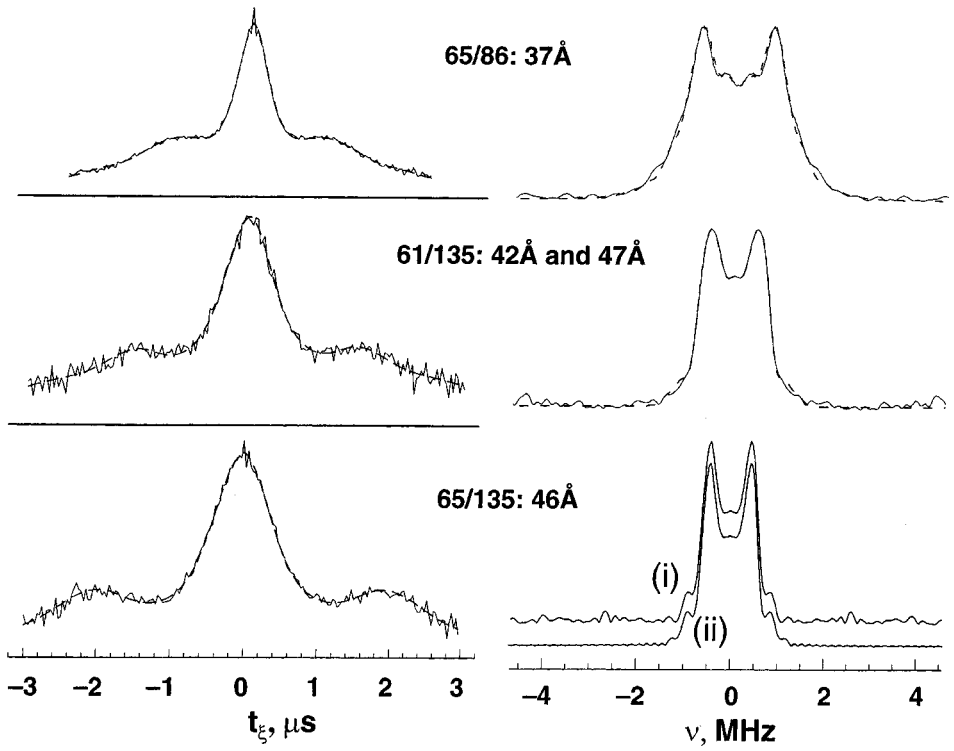

Figure 6. (Left column) DQC temporal envelopes (solid lines) after removal of the effects of nuclear spin diffusion (cf. Figure 4a) and their fits (dashed lines) for three T4L mutants with long distances: X-band and 77 K. (Right column) The dipolar spectra produced from Fourier transforming the experimental data, processed as described in the caption to Figure 4 and the text, and their fits. The simulated dipolar spectra are shown in dashed lines for 65/86 and 61/135. For 65/135, the experimental spectrum (i) is shifted upward with respect to its fit (ii).

Table 1. Distances and Distance Distributions for Two T4L Doubly Labeled Mutants from the DQC Experiments at Ku-band and at 204 K[a]

mutant	average distance, R_{av}, Å	ΔR, Å
65/76	21.4	2.8
65/80	26.5	3.8

[a] Here, R_{av} and ΔR are the parameters defined in Figure 10. They are obtained using model 1, for which ΔR is also the rms deviation.

Table 2. Distances and Distance Distributions for T4L Double Mutants from the DQC Experiments at X-band and at 77 K

mutant	average distance[a], R_{av}, Å	distribution width parameter[a], ΔR, Å	relative weight of component
65/135	46.3	2.2	
61/135	47.2	2.2	1
	41.8	1.6	2
65/86	37.4	2.7	
61/86	37.5	2.0	1
	33.5	2.2	2
61/80	34	2.2	1
	29	1.0	2
65/80	29.5	2.8	
80/135	36.8	1.0	

[a] Here R_{av} and ΔR are the parameters defined in Figure 10. They are obtained using model 1, for which ΔR is also the rms deviation.

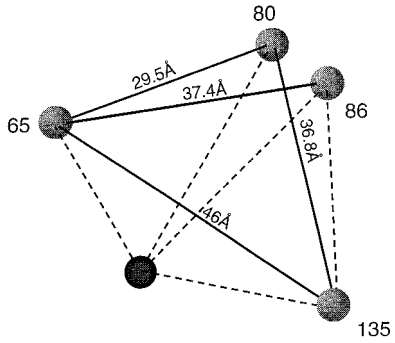

Figure 7. Distances obtained for some of the studied T4L doubly labeled mutants, showing the "triangulation" in progress. The gray spheres correspond to average widths of distributions found by fitting the DQC data. For the 86 mutant, there is insufficient data to fix its position with respect to the mutated sites shown. A dark sphere depicts a convenient location for a spin-labeled site, which would allow one to complete the tetrahedra forming a rigid 3-D mesh, as shown by dashed lines.

compare our results for R_{av} given in Table 2 with the distances $R_{\alpha\alpha}$ (and between the C_β's, i.e., $R_{\beta\beta}$) from the well-known crystal structure of T4L.[60]

We find that the differences between R_{av} and $R_{\alpha\alpha}$ range from 0 to about 10 Å. This is summarized in Table 3 for each mutant studied. In general, by our modeling procedure we can account for these differences as we describe shortly. We first note (as seen in Table 3) that the difference between $R_{\alpha\alpha}$ and $R_{\beta\beta}$ is an indication of the orientation of the secondary structure relative to the interspin vector $\mathbf{R_{av}}$. On the basis of this criterion, we may segregate the mutants into two groups. The first consists of pairs whose members are on the surface of the same helix, that is, helix C (these are mutants 61/80, 65/80, and 65/76, cf. Figure 2). In this case, there is little difference between $R_{\alpha\alpha}$ and $R_{\beta\beta}$. The second, consisting of the rest of the mutants, has $R_{\beta\beta}$ about 2.5 Å larger than $R_{\alpha\alpha}$ (except for 80/135). This second set of mutants probes the global fold of T4L (cf. Figure 2). It is expected that for the second group the linking arms will add significantly to R_{av}, whereas for the first group the linking arms

(60) Langen, R.; Oh, K. J.; Cascio, D.; Hubbell, W. L. *Biochemistry* **2000**, *39*, 8396.

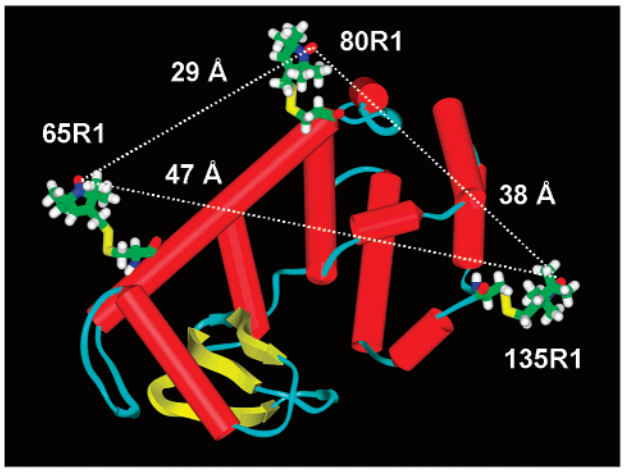

Figure 8. Molecular model of T4L showing nitroxide side chains at the three positions 65, 80, and 135. The triangulated distances shown are from the modeling (cf. text) and are in good agreement with the experimental results for R_{av} in Table 2.

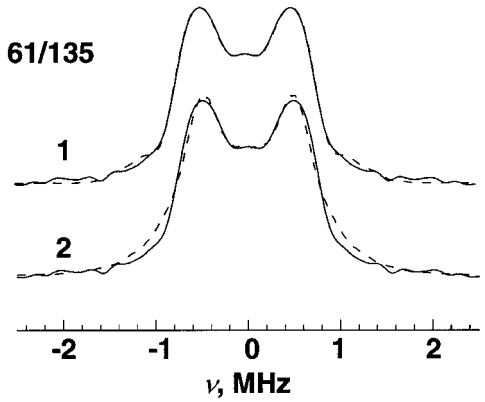

Figure 9. The dipolar spectrum for the mutant 61/135, obtained using two different models. (1) Fourier transformation of the experimental data from Figure 6 (solid line); the simulation with two components weighted in a 1:2 ratio: (i) $R_{av} = 47.2$ Å, $\Delta R = 2.2$ Å; (ii) $R_{av} = 41.8$ Å, $\Delta R = 1.6$ Å (dashed line). (2) Fourier transformation of the experimental data from Figure 6 (solid line). The simulation with use of a broad bell-shaped distribution (model 3): $R_{av} = 43$ Å, $\Delta R = 7$ Å (dashed line).

should be more nearly parallel, thereby contributing less to R_{av}. This is observed to be true for all cases (except 61/86).

Previous room-temperature ESR[54] and X-ray analysis[60] of R1-labeled mutants of T4L revealed the tendency of R1 to occupy a limited number of conformational states around the three bonds linking the C_α to the second sulfur (S_δ in Figure 1), with freer motion about the fourth and fifth bonds with dihedral angles labeled X4 and X5 in Figure 1.

By the choice of reasonable configurations for the R1 side chains, we can readily rationalize the measured distances (R_{av}) with the $R_{\alpha\alpha}$ and $R_{\beta\beta}$. It should be emphasized that in this effort we have just tried to demonstrate consistency between our present results on nitroxide−nitroxide distances and the known crystal structure. Thus, we have chosen one conformer for the first three bonds of the R1 side chain that was observed in the recent X-ray study.[60] We then used a molecular modeling routine (Insight-II Suite from Accelerys Inc.) to vary the value of X4, until agreement with experimental nitroxide distances was achieved. This implicitly assumes that X4, about which motion is possible at room temperature, exhibits a preferred value at 77 K, while X5 was allowed to be random (cf. next section on

Table 3. Comparisons of Average Distances between Nitroxides, R_{av}, from the DQC Experiments (cf. Table 2) with the Distances, $R_{\alpha\alpha}$ and $R_{\beta\beta}$, between the Respective α- and β-Carbons, Obtained from X-ray Crystallography[60]

mutant	R_{av}, Å	$R_{\alpha\alpha}$, Å	$R_{\beta\beta}$, Å	Δ^a, Å
61/80	34, 29	28.7	28.82	5.3, 0
65/80	28.0[b]	22.6	22.4	5
65/76	21.4	16.7	16.6	4.7
61/86	37.5, 33.5	34.4	37	3, 0.9
65/86	37.4	28.86	31.17	8.5
61/135	47.2, 41.8	37.7	40.43	9.5, 4
65/135	46.3	34.26	36.67	12
80/135	36.8	26.7	27.4	10

[a] $\Delta \equiv R_{av} - R_{\alpha\alpha}$. [b] Average of distances from X- and Ku-bands.

distributions). We wish to emphasize that while this procedure is a reasonable one, consistent with what is known about the R1 side chain and the protein structure, a different choice for the conformation of the first three bonds would likely lead to other reasonable structures in agreement with experiment. That is, we made no attempt to be exhaustive. Our results should just be taken as a demonstration that the values of R_{av} obtained in the present study are consistent with our knowledge of the T4L crystal structure.

The values of the dihedral angles that we used for the first three bonds are those of the $g^+g^+g^+$ rotamer reported by Langen et al., based on their crystallographic analysis of spin-labeled T4L.[60] They are for X1, X2, and X3: 300°, 300°, and 270°, respectively. We then found that a preferred value of 227° for X4 would simultaneously satisfy the 65/76 and 65/86 distances. However, to simultaneously satisfy the 65/135, 80/135, and 65/80 distances, while holding the X4 value at residue 65 fixed at 227°, it was necessary for X4 to prefer 159° for the spin-label at residue 80 and 340° for that at residue 135. There are two possible explanations for these different dihedral angles. They are either stabilized by local interactions of R1 with neighboring side chains, or else an alternative conformation to $g^+g^+g^+$ is adopted at the first three bonds, contrary to our modeling assumptions (cf. above). Consistent with the latter possibility is the fact that the backbone conformation at residue 135 is not helical (cf. Figure 8), unlike the 65, 76, and 86 sites. Also, the room-temperature ESR spectrum from a spin-label at residue 135 shows it to be highly mobile,[54] consistent with considerable conformational freedom that might include the first three bonds. The dihedral angle for the spin-label at the residue 80 does not differ as much as that for residue 135 from the others. This residue is the last in its helix (at the C-terminus), so it should deviate somewhat from a true helical state, again allowing for differences in the first three bonds of the R1 side chain.

Results from this procedure are illustrated in Figure 8 for the 65/80, 80/135, and 65/135 pairs of spin-labels. For these cases, the distances $R_{\beta\beta}$ were found to be 22.4, 27.4, and 36.7 Å, respectively, whereas those between the nitroxide spins (R_{av}) were 28.0, 36.8, and 46.3 Å, respectively. To account for these distances, the R1 side chains take on the geometries shown according to the procedure discussed above. This figure also further clarifies the "triangulation" approach of Figure 7.

What remains is to consider the mutants in which one of the labeled sites is 61. As we have already noted, these all show a bimodal distribution in Table 2. Here the shorter R_{av} is in two cases the same as $R_{\alpha\alpha}$ (i.e., 61/80 and 61/86) and just 4 Å greater in the third case (i.e., 61/135). Past ESR studies have shown

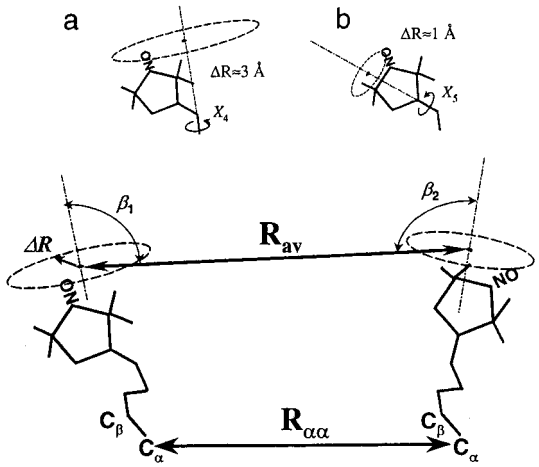

Figure 10. The geometrical arrangement of the two R1 side chains and the inter-nitroxide distances consistent with the X4/X5 model. This arrangement is used to calculate distance distributions, $P(r)$ between the nitroxides, where r is the inter-nitroxide distance. Here $R_{\alpha\alpha}$ is the distance between the two C_α carbons located on the backbone. Each circle with radius ΔR represents the possible locations of the nitroxide spins due to rotations about either the X4's or the X5's; R_{av} connects the centers of these two circles. The plane of each circle is referred to R_{av} by polar angles β_1 (circle 1) and β_2 (circle 2). Insets more clearly show a rotation about X4 and about X5.

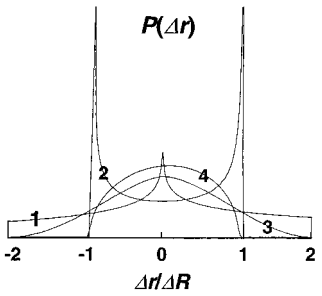

Figure 11. Model distance distributions, produced using the geometry of Figure 10, are depicted centered at the average distance R_{av}. Here $\Delta r \equiv r - R_{av}$. The following cases are shown: (1) β_1, $\beta_2 = 90°$ and uniform distributions on the circle circumferences; (2) $\beta_1 = 90°$, $\beta_2 = 0°$ (or vice versa) and uniform distributions on the circle circumferences; (3), (4) same angles as (1), (2), respectively, but with uniform distributions on the circles with radii ΔR.

two dramatically different spectral components with different mobilities when the 61 site is labeled.[54] The dominant component is the more ordered one. Thus, it is not at all unexpected that for all the pairs involving site 61, a bimodal distribution was obtained in our study. Also, in all cases, the shorter distance component is the more populous. A model consistent with this distance, and the fact that it is the more ordered one, is a conformation that has the nitroxide ring immobilized near the backbone. We note that since site 61 is at an N-terminus of the helix, this can be facilitated with H-bonding to the amide nitrogens. Finally, we do note that spectra from site 65 labeled with R1 also showed two components, but in this case their spectral differences were not very substantial.[54]

Distributions of Distance. As we have already pointed out, our fits to the DQC-ESR spectra provide not only R_{av}, but simultaneously information on the distribution in distances. That is, the shapes of the dipolar spectra are amenable to analysis in terms of distance distributions. In the future, this could be of potential value in providing insight on protein conformations, although our present results are consistent with the conformations of the R1 side chain being the dominant contributor to the observed distributions, as discussed below.

In our present studies, we have employed simple geometrical models reflecting general features of the R1 side chain referred to in the previous subsection. Again, we do not attempt to uniquely determine the structural features of the R1 chain that lead to the distributions, but rather to illustrate reasonable ones that provide a consistent interpretation of our results, and also illustrate the extent to which the DQC-ESR spectra can distinguish between different types of models.

The basis of our modeling of the distributions in r, where r is the inter-nitroxide distance, is illustrated in Figure 10 showing the orientations of the two R1 side chains relative to $\mathbf{R}_{\alpha\alpha}$. In this figure, $\mathbf{R_{av}}$ connects the centers of the circles swept out by the distributions of each R1 side chain. The radius of each such circle is ΔR. Clearly the distribution in r, or $P(r)$, is a function of the orientational distributions for each R1 side chain, as well as their orientations relative to $\mathbf{R_{av}}$. The plane of each circle (i.e., its normal) is referred to $\mathbf{R_{av}}$ by polar angle β. In the upper left (right) inset of Figure 10, we illustrate the specific case where the rotation is about X4 (X5). The general models based on Figure 10 that we use can account for either case or for both.

We have considered a variety of distributions and polar angles for each R1 side chain. We generated the combined distance distribution, $P(r)$ by a Monte Carlo method analogous to that used previously,[32] for each case. We show in Figure 11 some different cases that we generated, which illustrate the range of possibilities for $P(r)$ and also seem reasonably relevant to the structural features of the R1 side chains. In the first two cases, models 1 and 2, each nitroxide location sweeps out a cone, corresponding to being on the circumference of the circle with radius ΔR. This type of model is consistent with the molecular modeling involving rotations about X4 and/or X5. In model 1, both polar angles β are $\pi/2$, whereas in model 2, one is $\pi/2$, while the other is zero. We see that model 1 provides a fairly flat distribution ranging between $\pm 2\Delta R$ with a maximum at the center, whereas model 2 yields a narrower $P(r)$ ranging between $\pm\Delta R$ with two well-defined maxima at the end points. Both can be referred to as "box-type" distributions, and they are found to have root-mean-square (rms) deviations of ΔR and $\Delta R/\sqrt{2}$, respectively. [The rms deviation, Δr_{rms}, is given by $\langle (r - R_{av})^2 \rangle^{1/2}$.] Thus, Δr_{rms} changes significantly with β's (see below). For purposes of comparison, we also include models 3 and 4, wherein each nitroxide is allowed to take all points within the circle with equal probability. Model 3(4) has the same β values as those of model 1(2), hence the same range of values of r. Models 3 and 4, however, yield bell-shaped distributions $P(r)$ with Δr_{rms} of $\Delta R/\sqrt{2}$ and $\Delta R/2$, respectively.

Figure 12a illustrates, using models 1 and 2, how the dipolar spectra are affected by the particular model distributions of the same Δr_{rms}. As one can see, there are significant variations in the shape of the Pake doublets, which can readily be distinguished, given the good S/N achievable in the DQC experiments. [Figure 12b also shows that pseudosecular terms play a very minor role in affecting the dipolar spectra, as stated above in the subsection on distances.]

In general, we found that the distribution function, $P(r)$, associated with model 1 consistently provided the best fit to our results and so was used for the results reported in Table 2 (and Table 1). There is, as noted above, a preference for models

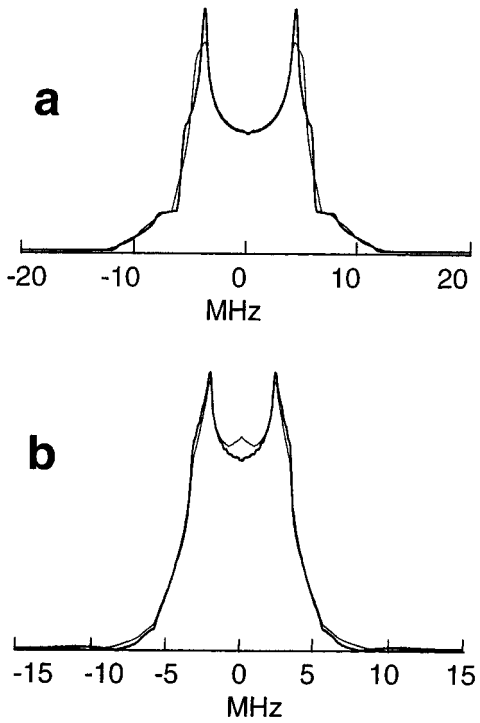

Figure 12. The shapes of dipolar spectra for model distributions (1) and (2) from Figure 11. (Panel a) The spectra for the distributions: (1) thin line, (2) thick line. Pseudosecular terms were omitted, R was 20 Å, ΔR was 1 Å for (1) and $\sqrt{2}$ Å for (2). Given the high S/N, such subtle differences in the dipolar spectra could be distinguished. (Panel b) The spectra for the distribution (2) simulated with (thin line) and without (thick line) the pseudosecular terms included. R_{av} was 25 Å, ΔR was 3 Å, and B_1 of 10 G was used in the calculations for uncorrelated ^{14}N nitroxides at X-band. It is clear that for the distances exceeding 25 Å (i.e., for all cases studied by X-band), pseudosecular terms do not have a significant effect on the dipolar spectra.

1 and 2 versus 3 and 4 based on the molecular modeling. Also, model 1 should be a more appropriate geometry (i.e., angles β), for the cases where both labels are on the surface of helix C, than is model 2. It is less obvious for the case of mutants that probe the global fold of T4L, but perhaps not unreasonable. We do wish to note that models 2−4 were able to provide reasonable fits for some of the mutants but not as consistently as model 1. Nor did they yield as consistent values of ΔR. Yet we regard our present results as insufficient to rule them out.

Whereas the molecular modeling shows that for motion about X4 and/or X5 the restriction to sweeping out the circumference of a circle is reasonable (i.e., models 1 and 2), free motion about both bonds would yield a ΔR of about 3 Å, while we typically obtain about 2.2−2.8 Å at 77 K. If we were to assume that X4 is fixed at a single orientation, while X5 is randomly distributed, this would lead to ΔR of ca. 1 Å. The reader will recall that the model we used to rationalize the observed values of R_{av} in terms of the known $R_{\alpha\alpha}$ suggested a preferred value of X4 for each mutant. The results on distance distributions using model 1 are consistent with this picture provided that there is just partial restriction of motion about X4 with a favored range of orientations.

Again, we must invoke the caveat that we have not exhaustively considered the extensive possibilities. In particular, a knowledge of the polar angles β would be helpful in determining distances between the points of attachment and properly rationalizing the distributions obtained from fitting the Pake doublets. Thus, for example, if instead of angles β of $\pi/2$ of model 1, we reduced β, then to fit a given experimentally observed Δr_{rms}, we would have to increase ΔR. This is the case for model 2, where one of the angles β is zero, since its Δr_{rms} equals $\Delta R/\sqrt{2}$ [instead of ΔR for model 1, cf. above]. The dependence of Δr_{rms} on angles β may be obtained by the Monte Carlo method we used to generate the $P(r)$. It is easier, however, to just consider the full range of $P(r)$, since it goes as $r_{max} - r_{min} \approx \Delta R(|\sin \beta_1| + |\sin \beta_2|)$ for $\Delta R \ll R_{av}$, and to recognize that Δr_{rms} will decrease monotonically as $r_{max} - r_{min}$ decreases, thereby requiring an increase in ΔR. It is clear that a larger ΔR would allow for greater freedom for X4 (hence the need for a somewhat different model used to rationalize the R_{av}). It would, therefore, be useful to obtain experimental information on the orientation of the nitroxide moiety relative to $\mathbf{R_{av}}$, which should be possible with a 2-D version of the DQC experiment[35] aided by use of more conformationally restricted labels.[54,61]

While we obtained values of ΔR of about 2 Å at 77 K, it appears from Table 1 that ΔR is a little larger at 204 K (from Ku-band), which we have already noted is to be expected at the higher temperature (cf. the 65/80 pair), but we need more extensive temperature-dependent results. The cases involving labeling at the 61 site, which give rise to a bimodal distribution at 77 K as discussed above, tend to show a smaller ΔR of less than 2 Å for the shorter distance, more populous, component. This would be consistent with the suggested model for this component involving immobilization near the backbone as discussed above.

We wish to point out at this juncture that the models we have been considering result in at least partial randomization of the orientation of the nitroxide moiety relative to the $\mathbf{R_{av}}$, and this is consistent with the assumption we made in our simulations (as discussed in the Data Analysis section) of no correlations in the respective orientations. A more thorough analysis of this matter awaits further experiments such as those utilizing the 2-D version of the DQC experiment, noted above.

Concluding Remarks

This study, using doubly labeled mutants of T4L, has clearly demonstrated the ability of the DQC-ESR method to yield distances in proteins in the range of 20 to 50 Å. This is a distance range that is not accessible by cw-ESR means. It is, however, a range that is valuable for the structure of large proteins and protein complexes. Also, as the distances between backbone sites that are labeled become longer, the uncertainty in their separation due to the length and flexibility of the side chains tethering the nitroxides becomes relatively less important. The DQC-ESR technique leads to dipolar spectra with excellent signal-to-noise that is largely free of artifacts. This leads to accurate distance determinations and to distance distributions, which we have shown in the present study to be consistent with the known crystal structure of T4L, the characteristic conformers of the side chain, and molecular modeling.

This study strongly implies that DQC-ESR can be used to detect triggered conformational transitions in proteins that involve rigid body movements. A particularly important application would be the observation of distance changes in the range not accessible to cw-ESR. For example, pH-gating of the

(61) Columbus, L.; Kálai, T.; Jekö, J.; Hideg, K.; Hubbell, W. L. *Biochemistry* **2001**, *40*, 3828.

bacterial potassium channel, KscA, involves relative movement of helices with a final separation that exceeds the 20 Å range detectable by cw line shape analysis.[62]

Given the high quality of the dipolar spectra that we are able to achieve, the methodology would benefit most from improvements stemming from the use of spin-labels of more limited flexibility and well-defined conformations.[61] There is every reason to believe that DQC-ESR can be utilized to study even longer distances,[63] as well as even smaller concentrations than the 250−500 μM samples used in this work[35] to those comparable to cw studies (ca. 50−100 μM) on shorter distances, thereby extending the range of its utility in protein structure determinations.

Acknowledgment. This work was supported by NIH/NCRR and NIH/GM grants, NSF grant CHE0098022, and NEI R2912018 and NEI R0112683 grants.

JA020040Y

(62) Perozo, E.; Cortes, D. M.; Cuello, L. G. *Science* **1999**, *285*, 73.

(63) Theoretical estimates[35] for DQC-ESR have indicated a maximum of 60 Å with protonated solvents, but 80 Å (or greater) was estimated to be possible with deuterated solvents, which suppress the effects of nuclear spin-diffusion.[35] Because we have studied distances <50 Å in this work, we found protonated solvents convenient and adequate.